Journal of Solid State Chemistry 184 (2011) 1141–1147

Contents lists available at ScienceDirect

Journal of Solid State Chemistry

journal homepage: www.elsevier.com/locate/jssc

A series of POM-based entangled frameworks with the rigid ligand 1,4-bis (1-imidazolyl)benzene and different isomers of octamolybdate

Hong-Ying Zang, Dong-Ying Du, Shun-Li Li, Ya-Qian Lan*, Guang-Sheng Yang, Li-Kai Yan, Kui-Zhan Shao, Zhong-Min Su*

Institute of Functional Material Chemistry, Key Laboratory of Polyoxometalate Science of Ministry of Education, Faculty of Chemistry, Northeast Normal University, Changchun 130024, People's Republic of China

ARTICLE INFO

Article history:
Received 26 December 2010
Received in revised form
19 February 2011
Accepted 27 February 2011
Available online 8 March 2011

Keywords:
Polyoxometalates
Octamolybdate
Entanglement
Semiconductor
Transition-metal ions

ABSTRACT

With BIMB ligand, we have successfully obtained and characterized three novel entangled inorganic–organic hybrid compounds by choosing different metal ions, that is, $[Ni(BIMB)_2(\gamma\text{-}Mo_8O_{26})_{0.5}]\cdot 3H_2O$ (**1**), $[Zn(BIMB)_2(\gamma\text{-}Mo_8O_{26})_{0.5}]$ (**2**), and $[Cu_3(BIMB)_4(H_2O)(\delta\text{-}Mo_8O_{26})Cl_2]\cdot 3H_2O$ (**3**) (where BIMB=1,4-bis(1-imidazolyl)benzene). Compound **1** is a 2-fold interpenetration 4-connected 3D framework with the short Schläfli symbol of $(4\times6^4\times8)_2(4^2\times6^2\times8^2)$, in which octamolybdate anion shows γ-isomer; 2 exhibits a (5,6)-connected 3D self-penetrating topological motif with the short Schläfli symbol of $(4\times5^7\times6^2)_2(4^2\times5^{11}\times7^2)$, and 3 shows a (4,6)-connected self-penetrating 3D framework with the short Schläfli symbol of $(4^2\cdot5^2\cdot6\cdot7)$ $(4^4\cdot5\cdot6^9\cdot8)$ $(5^4\cdot6^2)$ whose octamolybdate has δ-isomer. In addition, the optical band gaps of these three compounds have been measured, which are 2.98 eV for **1**, 3.42 eV for **2**, and 2.88 eV for **3**. Moreover, **2** has photoluminescent property, which can be attributed to ligand-to-metal charge-transfer (LMCT) band.

1. Introduction

Polyoxomolybdates have been on the stage not only due to their enchanting structural particularities such as a controllable shape, size, high-negative charge, and nucleophilic oxygen-enriched surface, but also due to various potential applications in catalysis, medicine, redox chemistry, and functional material science [1–4]. Moreover, the design and synthesis of POM-based materials 'on demand' is becoming increasingly important [5–9]. Introduction of polyoxoanions into inorganic–organic hybrid materials will make versatile intriguing structures, and more importantly, will multiply the functions of the compounds.

Further, entangled systems, one of the major themes of supramolecular chemistry, are common in biology—categorized as catenanes, rotaxanes, and molecular knots [10]—and have attracted considerable attention due to their esthetic and often complicated architectures and topologies [11,12]. According to Batten and Robson [13], interpenetrating network structures can be regarded as infinite, ordered polycatenanes or polyrotaxanes. The selection of the special ligand is very important in the construction of such entangled coordination polymers. Most frequently, the flexible ligands, such as 1,3-bis(4-pyridyl)propane [14,15], attract interest, as they exhibit flexibility and conformational freedom, which allow them to conform to the coordination environment of the metal ions and polyoxoanions, in favor of the construction of high dimensional and interpenetrating structures with intriguing topologies [16–19], while the rigid N-donor ligands are usually called 'terminator' for assembly of interpenetrating structures [20]. However, rigid ligand has predictable coordination conformation; furthermore, 1,4-bis(1-imidazolyl)benzene (BIMB) has a more flexible coordination fashion and an excellent coordination ability, and has already proven a certain ability to give interpenetrating networks in the previous works [21,22]. More importantly, this ligand can derive γ-$[Mo_8O_{26}]^{4-}$ for its imidazole units [23–25]. In light of this, it is highly possible for BIMB to play a 'two birds with one stone' role in the network construction. Octamolybdate never fails to appeal to chemists for its versatile isomers, that is, α-isomer, β-isomer, γ-isomer, δ-isomer, ε-isomer, ζ-isomer, η-isomer, and θ-isomer [26], prompt the formation of intriguing structures.

Herein, based on BIMB ligands, we have successfully obtained three novel entangled inorganic–organic hybrid compounds by choosing different metal ions. It is worth to mention that in these compounds, the octamolybdate shows γ and δ isomers and they act as multiple coordination positions.

2. Experimental

2.1. Materials and methods

All chemicals of reagent grade were purchased from commercial sources and used without further purification. 1,4-bis

* Corresponding author.
E-mail addresses: lanyq176@nenu.edu.cn (Y.-Q. Lan), zmsu@nenu.edu.cn (Z.-M. Su).

0022-4596/$ - see front matter © 2011 Published by Elsevier Inc.
doi:10.1016/j.jssc.2011.02.026

(1-imidazolyl)benzene (BIMB) ligand was synthesized by the method described in the literature [22,27]. Elemental analyses (C, H, and N) were performed on a Perkin-Elmer 240C elemental analyzer. The Fourier transform infrared (FT-IR) spectra were recorded from KBr pellets in the range 4000–400 cm^{-1} on a Mattson Alpha-Centauri spectrometer. Thermogravimetric analysis (TGA) was performed on a Perkin-Elmer TG-7 analyzer heated from room temperature to 800 °C under nitrogen at a rate of 10 °C min^{-1}. Diffuse reflectance spectra were measured on a finely ground sample with a Cary 500 spectrophotometer equipped with a 110 mm diameter integrating sphere. Solid-state fluorescence spectra were measured on a Cary Eclipse spectrofluorometer (Varian) equipped with a xenon lamp and quartz carrier at room temperature.

2.2. Syntheses

2.2.1. Synthesis of $[Ni(BIMB)_2(Mo_8O_{26})_{0.5}]\cdot 3H_2O$ (**1**)

The mixture of $(NH_4)_6Mo_7O_{24}\cdot 4H_2O$ (0.13 g, 0.10 mmol), BIMB (0.042 g, 0.2 mmol), and $Ni(NO_3)_2\cdot 6H_2O$ (0.030 g, 0.10 mmol) was stirred at room temperature for half an hour, and pH of the system was tuned to 5.0. The resulting suspension was transferred to a Teflon-lined stainless autoclave (25 mL) and kept at 160 °C for 72 h. Then it was cooled to 100 °C at a rate of 5 °C h^{-1}, held for 8 h, and followed by further cooling to 30 °C at a rate of 3 °C h^{-1}. Green crystals of **1** were collected in 56% yield based on $Ni(NO_3)_2$. Elemental Anal. Calcd for $C_{24}H_{26}Mo_4N_8NiO_{16}$ (1124.95): C, 25.62; H, 2.33; N, 9.96; Found: C, 25.59; H, 2.36; N, 9.92%. IR (cm^{-1}): 3134 (w), 1620 (w), 1527 (m), 1450 (w), 1260 (w), 1125 (m), 1056 (m), 945 (m), 900 (m), and 651 (m).

2.2.2. Synthesis of $[Zn(BIMB)_2(Mo_8O_{26})_{0.5}]$ (**2**)

The mixture of $(NH_4)_6Mo_7O_{24}\cdot 4H_2O$ (0.25 g, 0.20 mmol), BIMB (0.042 g, 0.2 mmol), and $Zn(NO_3)_2\cdot 6H_2O$ (0.020 g, 0.05 mmol) was stirred at room temperature for half an hour and pH value being 5.9. The resulting suspension was transferred to a Teflon-lined stainless autoclave (25 mL) and kept at 160 °C for 72 hours. Then it was cooled to 100 °C at a rate of 5 °C h^{-1}, held for 8 h, and followed by further cooling to 30 °C at a rate of 3 °C h^{-1}.Colorless crystals of **2** were collected in 50% yield based on $Zn(NO_3)_2$. Elemental Anal. Calcd for $C_{24}H_{20}N_8O_{13}ZnMo_4$ (1077.61): C, 26.75; H, 1.87; N, 10.40; Found: C, 26.73; H, 1.89; N, 10.38%. IR (cm^{-1}): 2972 (w), 1775 (m), 1689 (m), 1575(w), 1517 (s), 1453 (w), 1305 (w), 1126 (m), 935 (m), 861 (m), 712 (w), 649 (m), and 596 (m).

2.2.3. Synthesis of $[Cu_3(BIMB)_4(H_2O)(Mo_8O_{26})Cl_2]\cdot 3H_2O$ (**3**)

The synthesis of **3** was similar to **2** except that $CuCl_2\cdot 6H_2O$ (0.05 g, 0.2 mmol) substitutes $Zn(NO_3)_2\cdot 6H_2O$. Blue crystals of **3** were collected in 56% yield based on $CuCl_2$. Elemental Anal. Calcd for $C_{48}H_{44}Cl_2Cu_3\ Mo_8N_{16}O_{30}$ (2350.00): C, 24.51; H, 1.89; N, 9.54; Found: C, 24.54; H, 1.86; N, 9.56%. IR (cm^{-1}): 3342 (m), 1629 (w), 1529(sh), 1309 (w), 1068 (m), 958 (m), 830 (m), 651 (w), and 454 (m).

2.3. X-ray crystallographic study

Single-crystal X-ray diffraction data collection of the compounds was performed on a Bruker Smart Apex II CCD diffractometer with graphite-monochromated Mo Kα radiation (λ=0.71069 Å) at room temperature. All absorption corrections were performed using the SADABS program. All the four crystal structures were solved by the Direct Method of SHELXS-97 [28] and refined with full-matrix least-squares techniques (SHELXL-97) [29] within WINGX [30]. Anisotropic thermal parameters were employed to refine all non-hydrogen atoms. The hydrogen atoms of organic ligands were fixed at idealized positions as rigid groups. In compounds **1** and **3**, H atoms of water molecules could not be introduced in the refinement but were included in the structure factor calculation. The detailed crystallographic data and structure refinement parameters are listed in Table 1. Crystallographic data for the structures reported in this paper have been deposited in the Cambridge Crystallographic Data Center with CCDC reference numbers 777261, 777262, and 777263 for **1**, **2**, and **3**, respectively.

Table 1
Crystal data and structure refinement for **1**–**3**.

	1	**2**	**3**
Formula	$C_{24}H_{26}N_8O_{16}Mo_4Ni$	$C_{24}H_{20}N_8O_{13}ZnMo_4$	$C_{48}H_{44}N_{16}O_{30}Cl_2Cu_3Mo_8$
Formula weight	1124.95	1077.61	2350.00
Space group	$P\bar{1}$	$P2_1/n$	$P\bar{1}$
a (Å)	11.6690(11)	12.4840(10)	12.756(3)
b (Å)	12.5050(12)	15.9310(12)	12.809(3)
c (Å)	13.4300(13)	16.1670(13)	13.384(3)
α (deg.)	88.8020(14)	90	62.061(2)
β (deg.)	77.4430(12)	96.7000(10)	62.082(2)
γ (deg.)	65.8150(12)	90	83.306(3)
ρ_{cald} (gcm^{-3})	2.136	2.241	2.306
V ($Å^3$)	1739.8(3)	3193.4(4)	1692.2(6)
Z	2	4	1
F(0 0 0)	1088	2088	1137
Reflns collcd/unique	8825/6031	15975/5612	8322/5833
GOF on F^2	1.072	0.998	1.037
R_1[a] [$I>2\sigma(I)$]	0.0392	0.0395	0.0451
wR_2[b]	0.1115	0.0914	0.1296

[a] $R_1=\Sigma||F_o|-|F_c||/\Sigma|F_o|$.
[b] $wR_2=|\Sigma w(|F_o|^2-|F_c|^2)|/\Sigma|w(F_o^2)^2|^{1/2}$.

3. Results and discussion

3.1. Structural description

3.1.1. Structure of $[Ni(BIMB)_2(Mo_8O_{26})_{0.5}]\cdot 3H_2O$ (**1**)

By combining $Ni(NO_3)_2\cdot 6H_2O$, BIMB and $(NH_4)_6Mo_7O_{24}\cdot 4H_2O$, we successfully obtained a 3D γ-octamolybdate-based inorganic–organic hybrid compound, which crystallizes in triclinic space group $P\bar{1}$. X-ray crystallographic analysis reveals that there is unique kind of nickel ion, which is six-coordinated by three N atoms from different BIMB ligands, two water molecules and one oxygen atom from the octamolybdate anion (Fig. 1a). Further, the octamolybdate anion shows γ-isomer, which contains two {MoO_5} units and six {MoO_6} units, and the terminal oxygen atoms from {MoO_6} units bind to nickel ions in **1** (Fig. 1b). The nickel ions are interlinked by BIMB ligands to generate a flying-strand-like metal-organic chain. In addition, thanks to $[Mo_8O_{26}]^{4-}$ anions, two six-membered rings from distinct frameworks are catenated with each other (Fig. 1c). The hybrid compound features a 3D→3D parallel interpenetrated framework motif. Above all, octamolybdate anions and nickel cations can both be abstracted as four-connected nodes so as to simplify the whole structure as a 2-fold interpenetration 4-connected 3D framework with the short Schläfli symbol of $(4\times6^4\times8)_2(4^2\times6^2\times8^2)$. The unusual topological feature of compound **1** consists of the fact that the 2-fold interpenetrated frameworks are further catenated to the three adjacent (“upper” and “lower”) sheets in a parallel fashion to give an overall unique 3D framework (Fig. 1d).

3.1.2. Structure of $[Zn(BIMB)_2(Mo_8O_{26})_{0.5}]$ (**2**)

As is confirmed by X-ray crystallography, compound $[Zn(BIMB)_2(Mo_8O_{26})_{0.5}]$ (**2**) consists of two kinds of subunits: $[Zn(BIMB)_2]_n^{2n+}$ metal-organic cations and γ-$[Mo_8O_{26}]^{4-}$ anions. In compound **2**,

there exists one kind of crystallographically unique five-coordinated Zn^{II} cation surrounded by three N atoms from three BIMB ligands, two terminal O atoms from γ-$[Mo_8O_{26}]^{4-}$ anions, showing a distorted hexahedron coordination geometry (Fig. 2a). First, BIMB ligands connect Zn^{II} cations to construct a metal-organic chain like a cosine curve, and then the chain extends to a 2D network via BIMB ligands and γ-$[Mo_8O_{26}]^{4-}$ anions, and thanks to the multiple oxygen atoms of γ-$[Mo_8O_{26}]^{4-}$ (Fig. 2b), which connect Zn^{II} cations, the structure extends to a 3D framework (Fig. 2c, S1). When a Zn^{II} cation is regarded as a five-connected node and the γ-$[Mo_8O_{26}]^{4-}$ anion as a six-connected node, we obtained a (5,6)-connected topological structure with the short Schläfli symbol of $(4\times5^7\times6^2)_2(4^2\times5^{11}\times7^2)$ (Fig. 2d). More fascinatingly, this framework displays a self-penetrating phenomenon, that is, the shortest four-membered rings are catenated by the six-membered rings belonging to the same framework giving rise to a self-catenated motif (Fig. 2d, S1b). To the best of our knowledge, POM-based self-catenated coordination networks are unusual especially with rigid ligands. Most polycatenane motifs depend either on flexible organic ligands [14] or rotable inorganic building blocks [31]. Compound **2** enlightens us that rigid ligand and 'hard' inorganic building blocks can also construct self-catenated framework.

3.1.3. *Structure of $[Cu_3(BIMB)_4(H_2O)(Mo_8O_{26})Cl_2]\cdot 3H_2O$ (**3**)*

When using $CuCl_2$, a new self-penetrating compound containing Cu^{II} cations was achieved. Compound **3** is constructed from δ-$[Mo_8O_{26}]^{4-}$ clusters, and $[Cu^{II}(BIMB)_2Cl_2]_n$ and $\{[Cu^{II}_2(BIMB)_2]_n\}^{4n+}$ metal-organic motifs. There exist two kinds of crystallographically unique Cu^{II} cations, the coordination geometries of which are shown in Fig. 3a: the Cu1 atom is surrounded by four N atoms from four BIMB ligands (Cu(1)–N(1)=1.993(5) and Cu(1)–N(3)=1.998(5) Å) and two O atoms from two δ-$[Mo_8O_{26}]^{4-}$ anions (Cu(1)–O(12)=2.530(5) Å), showing a distorted octahedral geometry; the Cu2 atom is also six coordinated and is surrounded by two N atoms from BIMB ligand, two Cl^- anions, one water molecule, and one O atom from $[Mo_8O_{26}]^{4-}$ anion (Cu(2)–N(5)=1.974(6), Cu(2)–N(7)=1.955(6), Cu(2)–Cl(1)=2.306(2), Cu(2)–Cl(1#a)=2.819(2), Cu(2)–O2W=2.062(6), and Cu(2)–O(10)=2.665(6) Å) (Table S3). In this compound, the octamolybdate anion shows δ type, which contains four $\{MoO_5\}$ and four $\{MoO_6\}$ units (Fig. 3b) and the δ-$[Mo_8O_{26}]^{4-}$ coordinates to four Cu atoms. Intriguingly, the $\{[Cu^{II}_2(L^2)_2]_n\}^{4n+}$ motif constructs a 2D network, and $[Cu^{II}(L^2)_2Cl_2]_n$ motif threads through the 2D grids like 'sugar-coated haws on a stick' (Fig. 3c). Meanwhile, adjacent metal-organic grids are extended by δ-$[Mo_8O_{26}]^{4-}$ anions through Cu–O interaction giving rise to a 3D framework (Fig. 3d). Similarly, we previously reported two supramolecular isomerism with a polythreaded topology based on octamolybdate building blocks via Cu–O interaction [32]. More fascinatingly, because of the voids in this framework, it displays a unique self-penetrating phenomenon, that is, the six-membered rings are catenated by the four-membered rings from another inclined layer belonging to the same framework so as to give rise to a (4,6)-connected self-penetrating polycatenane motif

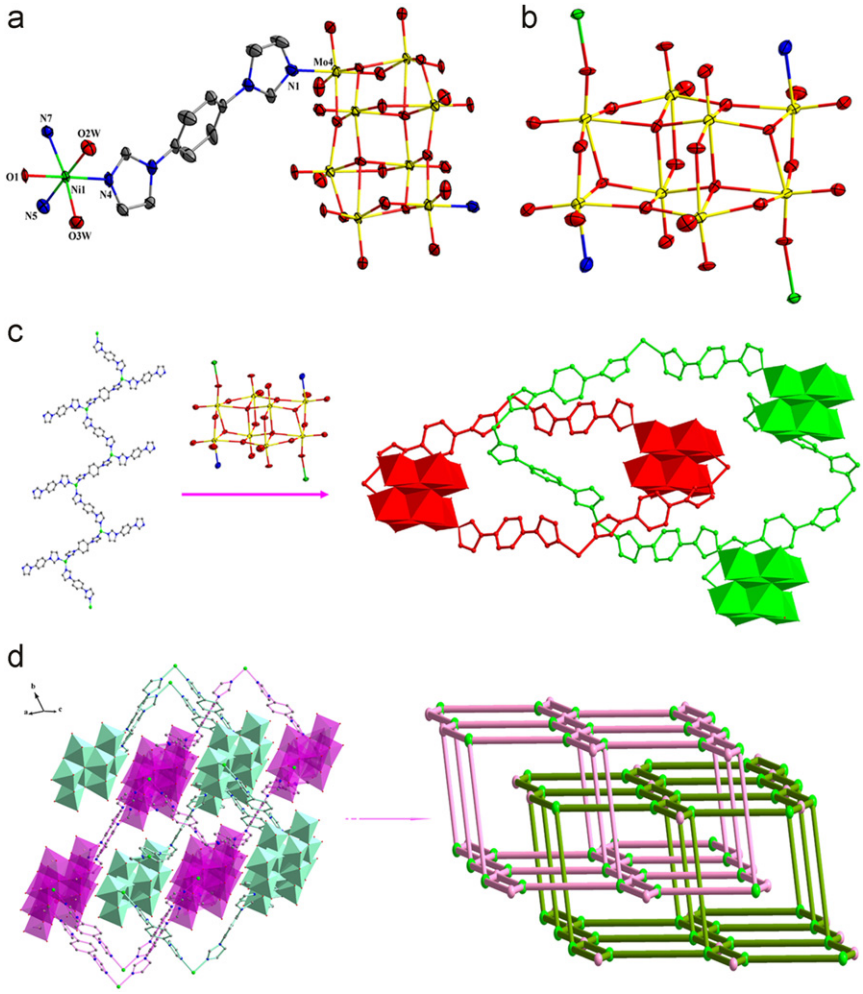

Fig. 1. (a) Coordination mode of Ni^{II} in compound **1** with 50% thermal ellipsoids. All hydrogen atoms were omitted for clarity. (b) Coordination mode of γ-octamolybdate isomer. (c) View of packing of the framework in **1** along *b* axis. (d) Topological representation of 2-fold interpenetration 4-connected 3D framework.

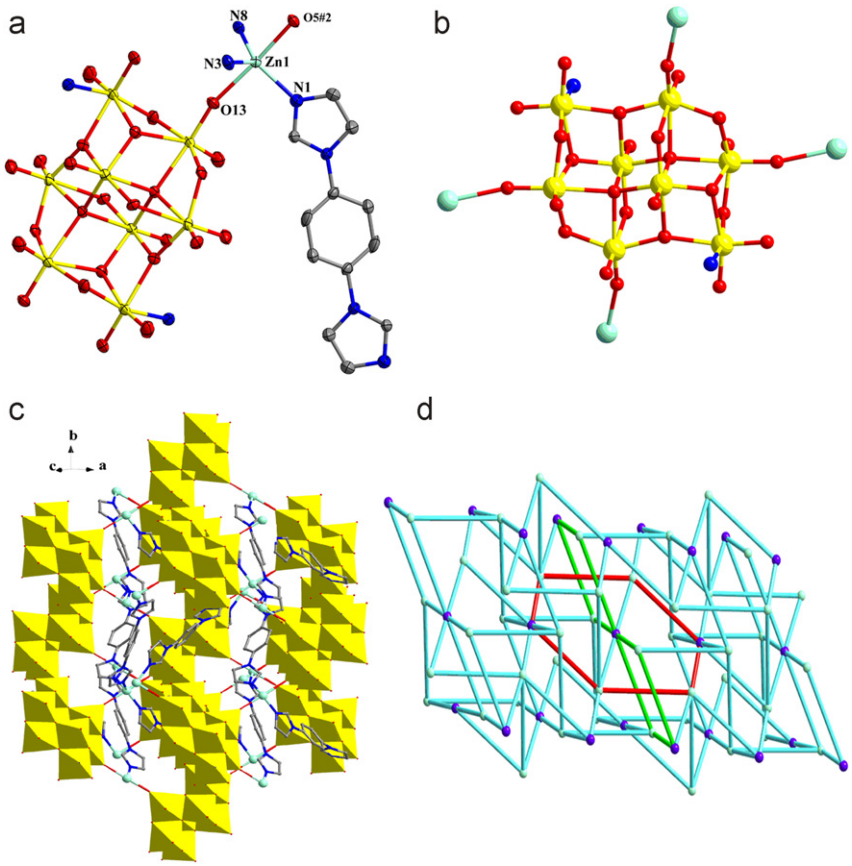

Fig. 2. (a) Coordination mode of Zn^{II} in compound **2** with 50% thermal ellipsoids. All hydrogen atoms were omitted for clarity. (b) Coordination mode of γ-octamolybdate isomer. (c) View of cobweb-like framework along *c* axis. (d) Topological representation of the (5,6)-connected framework, and the light blue and purple circles represent zinc and γ-$[Mo_8O_{26}]^{4-}$, respectively. (For interpretation of the references to color in this figure legend, the reader is referred to the web version of this article.)

with the short Schläfli symbol of $(4^2 \times 5^2 \times 6 \times 7)$ $(4^4 \times 5 \times 6^9 \times 8)$ $(5^4 \times 6^2)$ (Fig. 3e).

3.2. Overview

Based on BIMB ligands, three new octamolybdate-based compounds with entanglement frameworks have been synthesized after changing pH values and metal ions. As reported previously, the pH value of the reaction system is crucial for the formation of the different isomers [21,33]. We obtained γ type at lower pH value 4.0 and δ type at 6.0. In compounds **1** and **2**, the octamolybdate anion shows γ-isomer, while in **3** it shows δ-isomer (Fig. S2). Moreover, different metal ions have different coordination geometry and different affinity to octamolybdate anions. Compound **1** is a 3D 4-connected interpenetrating polycatenane framework, in which Ni^{II} cations and γ-$[Mo_8O_{26}]^{4-}$ anions can be regarded as four-connected nodes. Using Zn^{II} instead of Ni^{II}, a new type of polycatenane framework has been constructed; Zn^{II} can be regarded as a five-connected node and γ-$[Mo_8O_{26}]^{4-}$ coordinates to six Zn^{II} cations; so the whole framework exhibits a (5,6)-connected self-penetrating framework. Further, when we use Cu^{II} cations, the octamolybdate shows the δ-isomer seen as a four-connected node, and meanwhile, the Cu(1) atom is seen as a six-connected node and Cu(2) atom is deemed as a four-connected node. As a consequence, the framework is a (4,6)-connected novel self-penetrating motif. Above all, different metal ions not only exhibit various coordination modes but also influence the coordination modes of octamolybdate as well as the conformations of octamolybdate. Moreover, the frameworks of compounds are also greatly influenced.

3.3. Thermogravimetric analyses (TGA)

Thermal stability of compounds **1**–**3** has been investigated by means of TG analysis (Fig. S3). Compound **1** shows a two-step sequential weight loss: the first step happens between 54 and 170 °C corresponding to loss of lattice water molecules and on further heating the residue goes on decomposing till about 700 °C. Compound **2** is stable up to approximately 400 °C and undergoes sharp decrease till 700 °C. In compound **3**, the lattice water molecules and coordination water molecules lose before 300 °C (exptl., 2.82; calcd., 3.07%), and decomposition of the framework occurs at about 400 °C.

3.4. UV/vis/NIR diffuse reflectance spectra

Current research efforts have concentrated on the synthesis of heterometallic oxides/organics containing both early (V^{5+}, Mo^{6+}, and Re^{7+}) and late (Ni^{2+}, Cu^{2+}, Zn^{2+}, and Cu^{+}) transition metals in combination with structure-directing organic ligands that will coordinate preferentially to the late transition-metal sites [34,35]. This selection of early/late transition metals is useful for probing the structural and electronic origins of the band gap sizes of heterometallic oxides that arise from a Metal-to-Metal Charger Transfer (MMCT) [36]. As a consequence, the measurements of diffuse reflectance for powder samples were used to study the

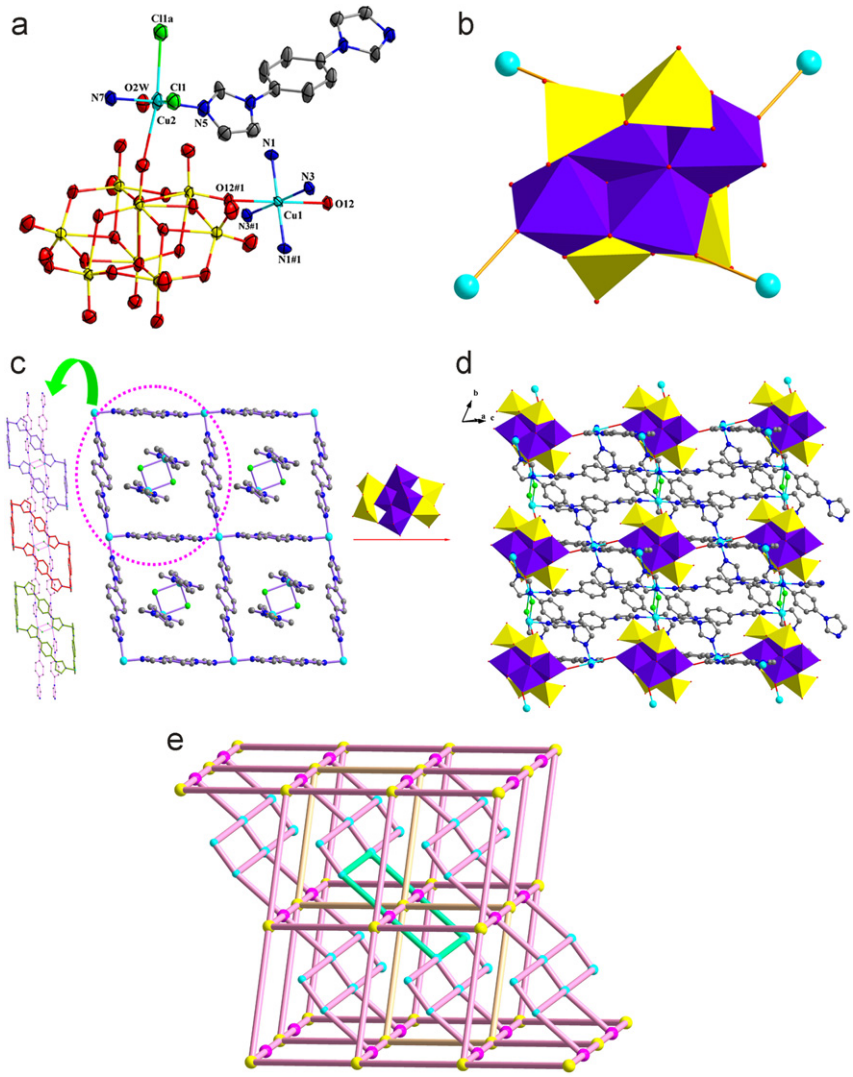

Fig. 3. (a) Coordination mode of Cu^{II} in compound **3** with 50% thermal ellipsoids. All hydrogen atoms were omitted for clarity. (b) Polyhedral representation of δ-$[Mo_8O_{26}]^{4-}$ anion and its coordinating mode. (c) Ball-and-stick representation of grid-like 2D network. More interestingly, the metal-organic framework itself exhibits a polythreading motif. (d) Ball-and-stick and polyhedral representation of the 3D framework. (e) Topological representation of the (4,6)-connected framework.

band gap (E_g), which is determined as the intersection point between the energy axis and the line extrapolated from the linear portion of the adsorption edge in a plot of Kubelka–Munk function F against E [37]. As shown in Fig. 4, the corresponding well-defined band gap (E_g) can be assessed at 2.98 eV for **1**, 3.42 eV for **2**, and 2.88 eV for **3**. The reflectance spectra indicate that the presence of comparatively wide energy gaps for these four compounds, which indicates that these hybrid compounds are potential wide gap semiconductor materials. The extended $[Ni(\gamma\text{-}Mo_8O_{26})_{0.5}]_n$, $[Zn(\gamma\text{-}Mo_8O_{26})_{0.5}]_n$, and $[Cu^{II}_2(\delta\text{-}Mo_8O_{26})]_n$ subunits in hybrid structures appear to be mainly responsible for their optical band gaps.

3.5. Photoluminescence for **2**

The luminescent properties of free ligand BIMB and the hybrid **2** were investigated in the solid state at room temperature, as depicted in Fig. S4 in the Supplementary Information. Compared with the maximum emission wavelength for the BIMB ligand at ca. 370 nm (λ_{ex}=322 nm), compound **2** exhibits a reduced photoluminescence emission at 455 nm (λ_{ex}=337 nm), showing an obvious red shift. The origin of the emission of compound **2** may be tentatively assigned to the ligand-to-metal charge-transfer (LMCT) band [38–43].

4. Conclusions

To sum up, we successfully synthesized a series of octamolybdate-based entanglement frameworks with the rigid ligand 1,4-bis(1-imidazolyl)benzene instead of usually used flexible ligands. In compounds **1** and **2**, the octamolybdate anions show the γ-isomer, and the whole structure exhibits a 2-fold interpenetration 4-connected 3D framework with the short Schläfli symbol of $(4\times6^4\times8)_2(4^2\times6^2\times8^2)$ and a (5,6)-connected 3D self-penetrating motif with the short Schläfli symbol of $(4\times5^7\times6^2)_2(4^2\times5^{11}\times7^2)$. While **3** shows a (4,6)-connected self-penetrating 3D framework with the short Schläfli symbol of $(4^2\times5^2\times6\times7)$ $(4^4\times5\times6^9\times8)$ $(5^4\times6^2)$ and the octamolybdate anion has a δ-isomer. In addition, we also investigated the optical band gap of these three compounds and the results show that they are all wide gap semiconductors, which are 2.98 eV for **1**, 3.42 eV for **2**, and 2.88 eV for **3**. Moreover, **2** exhibits

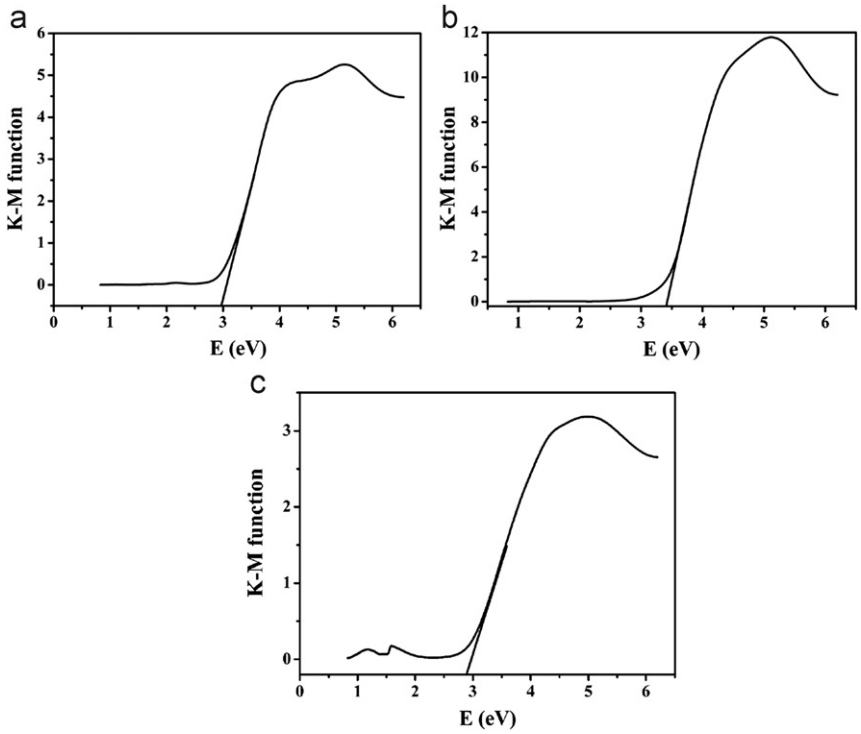

Fig. 4. Diffuse reflectance spectra of compounds **1**–**3**.

photoluminescence emission at 455 nm when excited at 337 nm. Its photoluminescent property can be attributed to ligand-to-metal charge-transfer (LMCT).

Acknowledgments

The authors gratefully acknowledge the financial support from the National Natural Science Foundation of China (nos. 20901014 and 21001020), the Science Foundation for Young of Jilin Scientific Development Project (nos. 20090125 and 20090129), the Fundamental Research Funds for the Central Universities (nos. 20090407 and NENU-STC08019), the Ph.D. Station Foundation of Ministry of Education for New Teachers (no. 20090043120004), the Postdoctoral Foundation of Northeast Normal University, the Postdoctoral Foundation of China (no. 20090461029), and the Special Grade of the Postdoctoral Foundation of China (no.201003528).

Appendix A. Supplementary material

Supplementary material associated with this article can be found in the online version at doi:10.1016/j.jssc.2011.02.026.

References

[1] C.L. Hill, Chem. Rev. 98 (1998) 1.
[2] A. Müller, C. Serain, Acc. Chem. Res. 33 (2000) 2.
[3] D.L. Long, E. Burkholder, L. Cronin, Chem. Soc. Rev. 36 (2007) 105.
[4] D.L. Long, R. Tsunashima, L. Cronin, Angew. Chem. Int. Ed. 49 (2010) 1736.
[5] P.J. Hagrman, R.L. LaDuca, H.J. Koo, R. Rarig, R.C. Haushalter, M.H. Whangbo, J. Zubieta, Inorg. Chem. 39 (2000) 4311.
[6] R. Vaidhyanathan, S. Natarajan, C.N.R. Rao, Dalton Trans. (2003) 1459.
[7] N. Snejko, C. Cascales, B. Gómez-Lor, E. Gutiérrez-Puebla, M. Iglesias, M.A. Monge, C. Ruiz-Valero, Chem. Commun. (2002) 1366.
[8] C. Streb, C. Ritchie, D.L. Long, P. Kögerler, L. Cronin, Angew. Chem. Int. Ed. 46 (2007) 7579.
[9] S.T. Zheng, J. Zhang, G.Y. Yang, Angew. Chem. Int. Ed. 47 (2008) 3909.
[10] J.P. Sauvage, C. Dietrich-Buchecker (Eds.), Molecular Catenanes, Rotaxanes and Knots: A Journey Through the World of Molecular Topology, Wiley-VCH, Weinheim, 1999.
[11] L. Carlucci, G. Ciani, D.M. Proserpio, Coord. Chem. Rev. 246 (2003) 247.
[12] X.H. Bu, M.L. Tong, H.C. Chang, S. Kitagawa, S.R. Batten, Angew. Chem. 116 (2004) 194 Angew. Chem. Int. Ed. 43 (2004) 192.
[13] S.R. Batten, R. Robson, Angew. Chem. 110 (1998) 1558 Angew. Chem. Int. Ed. 37 (1998) 1460.
[14] X.S. Qu, L. Xu, G.G. Gao, F.Y. Li, Y.Y. Yang, Inorg. Chem. 46 (2007) 4775.
[15] X.L. Wang, Y.F. Bi, B.K. Chen, H.Y. Lin, G.C. Liu, Inorg. Chem. 47 (2008) 2442.
[16] X.L. Wang, C. Qin, E.B. Wang, Z.M. Su, Chem. Commum. (2007) 4245.
[17] Y.Q. Lan, S.L. Li, Z.M. Su, K.Z. Shao, J.F. Ma, X.L. Wang, E.B. Wang, Chem. Commum. (2008) 58.
[18] B.X. Dong, J. Peng, C.L. Gómez-García, S. Benmansour, H.Q. Jia, N.H. Hu, Inorg. Chem. 46 (2007) 5933.
[19] A.X. Tian, J. Ying, J. Peng, J.Q. Sha, Z.G. Han, J.F. Ma, Z.M. Su, N.H. Hu, H.Q. Jia, Inorg. Chem. 47 (2008) 3274.
[20] A.X. Tian, J. Ying, J. Peng, J.Q. Sha, Z.M. Su, H.J. Pang, P.P. Zhang, Y. Chen, M. Zhu, Y. Shen, Cryst. Growth Des. 10 (2010) 1104.
[21] Y. Qi, Y.X. Che, J.M. Zheng, Cryst. Growth Des. 8 (2008) 3602.
[22] G.S. Yang, Y.Q. Lan, H.Y. Zang, K.Z. Shao, X.L. Wang, Z.M. Su, C.J. Jiang, Cyst. Eng. Commun. 11 (2009) 274.
[23] P. Gili, P.A. Lorenzo-Luis, A. Mederos, J.M. Arrieta, G. Germain, A. Castiñeiras, R. Carballo, Inorg. Chim. Acta 295 (1999) 106.
[24] C.D. Wu, C.Z. Lu, S.M. Chen, H.H. Zhuang, J.S. Huang, Polyhedron 22 (2003) 3091.
[25] K. Pavani, S.E. Lofland, K.V. Ramanujachary, A. Ramanan, Eur. J. Inorg. Chem. (2007) 568.
[26] H.Y. Zang, Y.Q. Lan, G.S. Yang, X.L. Wang, K.Z. Shao, G.J. Xu, Z.M. Su, Cyst. Eng. Commun. 12 (2010) 434.
[27] J. Fan, B.E. Hanson, Chem. Commun. (2005) 2327.
[28] G.M. Sheldrick, SHELXS-97, Programs for X-ray Crystal Structure Solution, University of Göttingen, Göttingen, Germany, 1997.
[29] G.M. Sheldrick, SHELXL-97, Programs for X-ray Crystal Structure Refinement, University of Göttingen, Göttingen, Germany, 1997.
[30] L.J. Farrugia, A. WINGX, Windows Program for Crystal Structure Analysis, University of Glasgow, Glasgow, U.K, 1988.
[31] R.F. Luis, M.K. Urtiaga, J.L. Mesa, A.T. Aguayo, T. Rojob, M.I. Arriortua, Cyst. Eng. Commun. 12 (2010) 1880.
[32] Y.Q. Lan, S.L. Li, X.L. Wang, K.Z. Shao, Z.M. Su, E.-B. Wang, Inorg. Chem. 47 (2008) 529.
[33] Q.-G. Zhai, R. Ding, S.-N. Li, W.-J. Ji, X. Gao, Y.-C. Jiang, M.-C. Hu, Inorg. Chim. Acta 363 (2010) 653.
[34] H. Kato, H. Kobayashi, A. Kudo, J. Phys. Chem. B 106 (2002) 12441.
[35] R. Konta, H. Kato, H. Kobayashi, A. Kudo, Phys. Chem. Chem. Phys. 5 (2003) 3061.

[36] B. Yan, M.D. Capracotta, P.A. Maggard, Inorg. Chem. 44 (2005) 6509.
[37] J.I. Pankove, Optical Processes in Semiconductors, Prentice-Hall, Inc., Englewood Cliffs, NJ, 1971, p. 34.
[38] G. Blasse, K.C. Bleijenberg, R.C. Powell, Structure and Bonding 42: Luminescence and Energy Transfer, Springer-Verlag, Berlin, 1980.
[39] G.A. Crosby, R.G. Highland, K.A. Truesedell, Chem. Rev. 64 (1985) 41.
[40] C. Kutal, Coord. Chem. Rev. 99 (1990) 213.
[41] G. Blasse, E. König, S.B. Padhye, P.B. Sonawane, D.X. West, Structure and Bonding, 76, Complex Chemistry, Springer-Verlag, Berlin, 1991.
[42] Z.R. Pan, Y. Song, Y. Jiao, Z.J. Fang, Y.Z. Li, H.G. Zheng, Inorg. Chem. 47 (2008) 5162.
[43] S.L. Zheng, J.H. Yang, X.L. Yu, X.M. Chen, W.T. Wong, Inorg. Chem. 43 (2004) 830.